2000

Fortnightly Variability in the Transverse Dynamics of a Coastal Plain Estuary

Arnoldo Valle-Levinson
Old Dominion University

Kuo-Chuin Wong

Kamazima M. M. Lwiza

Original Publication Citation

Valle-Levinson, A., & Wong, K. C. (2000). Fortnightly variability in the transverse dynamics of a coastal plain estuary. *Journal of Geophysical Research: Oceans, 105*(C2), 3413-3424. doi:10.1029/1999jc900307

JOURNAL OF GEOPHYSICAL RESEARCH, VOL. 105, NO. C2, PAGES 3413-3424, FEBRUARY 15, 2000

Fortnightly variability in the transverse dynamics of a coastal plain estuary

Arnoldo Valle-Levinson
Center for Coastal Physical Oceanography, Department of Ocean, Earth, and Atmospheric Sciences
Old Dominion University, Norfolk, Virginia

Kuo-Chuin Wong
College of Marine Studies, University of Delaware, Newark

Kamazima M.M. Lwiza
Marine Sciences Research Center, State University of New York, Stony Brook

Abstract. Current velocity and water density profiles were obtained along two cross-estuary transects with the purpose of determining the fortnightly variability of the transverse dynamics in a partially stratified coastal plain estuary. The profiles were measured with a towed acoustic Doppler current profiler and a conductivity-temperature-depth recorder in the James River estuary, Virginia. The cross-estuary transects were sampled during the spring tides of October 26-27, 1996, and the ensuing neap tides of November 2-3, 1996. The transects were ~4 km long, featured a bathymetry that consisted of a channel flanked by shoals, and were sampled repeatedly during two semidiurnal tidal cycles (25 hours) in order to separate semidiurnal, diurnal, and subtidal signals from the observations. This work concentrates on the subtidal transverse dynamics. The transverse baroclinic pressure gradients were larger during neap tides than during spring tides. During spring tides the advective accelerations were predominantly greater than the Coriolis accelerations, most markedly over the edges of the channel. Both effects combined with frictional influences to balance the pressure gradient in the transverse direction. During neap tides, advective accelerations were not as dominant over Coriolis accelerations as during spring tides. Also, during neap tides, Coriolis played a more relevant role, compared to spring tides, in combining with friction to balance the pressure gradient. This behavior was indicative of the momentum balance approaching gravitational circulation modified by the Earth's rotation, weak friction, and nonlinear advection during neap tides. The balance became more influenced by nonlinear advection and friction and less influenced by the Earth's rotation during spring tides. These results showed that transverse dynamics of a partially stratified estuary are far from being in geostrophic balance.

1. Introduction

Estuarine processes vary at diverse time scales that range from intratidal to interannual. It has been well documented that the fortnightly variability in tidal forcing may result in appreciable changes in stratification and subtidal flow [e.g., *Haas*, 1977; *Nunes and Lennon*, 1987; *Griffin and LeBlond*, 1990; *Jay and Smith*, 1990; *Simpson et al.*, 1990]. Increased stratification and subtidal along-estuary flows develop through enhanced gravitational circulation during neap tides relative to spring tides. These changes arise from the modulation by tidal mixing of the frictional accelerations that balance the pressure gradient accelerations in the along-estuary x momentum balance. The studies that document such fortnightly variability have been based on density and flow profiles measured at one location or a series of locations along the estuary, giving a two-dimensional (along-estuary x versus depth z) picture. The limitation of the two-dimensional picture was noted by *Fischer* [1972, 1976], who suggested that the transverse (or across-estuary y) structure of the along-estuary fields plays a crucial role in the mass transport in estuaries. Increased attention has concentrated on the transverse structure of the density and along-estuary mean flow fields [e.g., *Kjerfve*, 1978; *Kjerfve and Proehl*, 1979; *Huzzey and Brubaker*, 1988; *Wong*, 1994; *Wong and Münchow*, 1995; *Valle-Levinson and Lwiza*, 1995; *Friedrichs and Hamrick*, 1996]. However, the across-estuary mean flow fields, which provide the complete three-dimensional description of the estuary, customarily have been neglected.

In the transverse direction y the momentum balance in partially stratified estuaries has been usually assumed to be geostrophic, i.e., no flow in the across-estuary direction. This assumption is based on the work by *Pritchard* [1956] in

Paper number 1999JC900307.
0148-0227/00/1999JC900307$09.00

the James River, where he considered the influence of friction of secondary importance, even though the frictional terms were comparable to the Coriolis accelerations [*Pritchard*, 1956, Table III]. Because of the assumption of geostrophic dynamics in the transverse direction it has also been supposed that there is no fortnightly variability in the transverse dynamics of a partially stratified estuary. Recently, however, *Valle-Levinson and Atkinson* [1999] found that non-linear advection across the estuary can be of greater magnitude than the Coriolis accelerations in some portions of the lower Chesapeake Bay, thus invalidating the geostrophic assumption. Also, it is well known that around headlands [e.g., *Geyer*, 1993] and around meandering channels [e.g., *Bathurst, et al.*, 1977; *Thorne and Hey*, 1979; *Kalkwijk and Booij*, 1986; *Dronkers*, 1996] nonlinear effects in the form of centrifugal accelerations tend to dominate over Coriolis accelerations. Nonetheless, the later studies concentrated on the interaction of tidal currents with bathymetry over relatively short cross sections of systems with pronounced curvatures and, for the most part, vertically well mixed. The objectives of this study are (1) to assess the validity of the geostrophic approximation across an entire section of a partially stratified coastal plain estuary and (2) to explore the fortnightly variability of the transverse dynamics in a coastal plain estuary. This is done by calculating the magnitude of the terms in the transverse momentum balance that are assessable with velocity and density profiles obtained at two transects across the James River estuary, Virginia.

A description of the study area is presented in Section 2, followed by a presentation of the data collection and processing techniques in Section 3. Then, the fortnightly variability of the mean density and flow fields is discussed, followed by the presentation of the pressure gradients and their fortnightly variability in Section 4. The magnitude of these gradients is then compared to that of the Coriolis and advective accelerations and to the magnitude of the frictional or vertical exchange of momentum term. The main conclusions are presented in Section 5.

2. Study Area

The James River estuary is the southernmost tributary to the Chesapeake Bay. It has been chosen as the location to examine the objectives mentioned above because it is narrow enough to allow near-synoptic sampling of the density and flow fields (Figure 1). Also, this estuary is a typical example of a partially stratified coastal plain estuary and is where a large amount of the pioneering work on estuarine dynamics took place [*Pritchard* 1952, 1954, 1956]. In addition, the James River displays a bathymetry that consists of a main channel of maximum depth of 15 m, located approximately between 0 and 2 km from the beginning of each transect (Figure 1), and a secondary channel, 5-6 m deep, located roughly at 3 km from the beginning of each transect. The main channel is partitioned into a deep part (up to 15 m deep) and a shallow part (~9 m deep). In the deep part, between 0 and 1 km, flood currents are stronger than ebb currents (flood-dominated part) and in the shallow part, between 1 and 2 km, ebb currents are stronger than flood currents (ebb-dominated part). As will be seen, this partition of the main channel has relevant implications to the transverse dynamics of this system.

The study area is located over a relatively straight segment

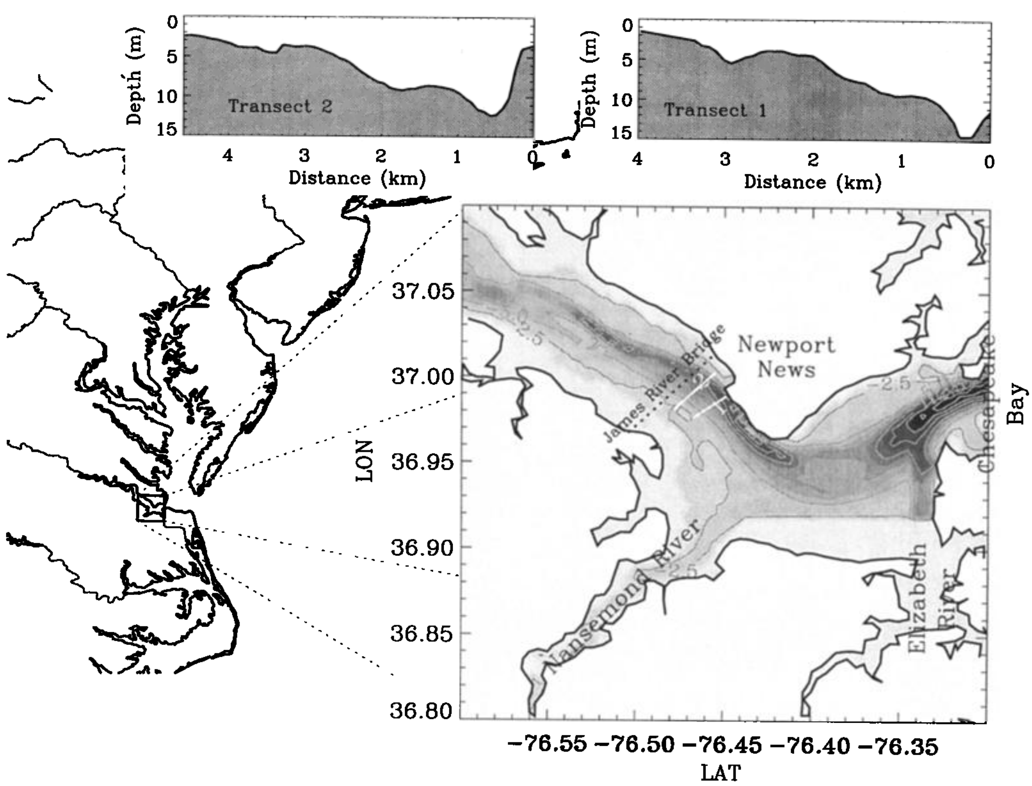

Figure 1. Map of the northeastern coast of the United States, showing an enlargement (bottom right) of the portion of the James River studied, within the lower Chesapeake Bay. Bathymetry is contoured at intervals of 2.5 m. The deepest part of the channel off Newport News is ~15 m. Transects 1 and 2 (white lines) are drawn to the south of the James River Bridge (dotted black line). The depth distribution of the transects is shown, looking into the estuary, in the inserts at the top.

(shorelines are roughly parallel) of the lower James River in the vicinity of the James River Bridge (Figure 1). The bridge structure should not significantly alter flow or stratification patterns in the area of the transects sampled. *Miller and Valle-Levinson* [1996] found that the bridge pilings of the Chesapeake Bay Bridge-Tunnel in the lower Chesapeake Bay altered stratification by <5% and only within 200 m from the structure. On the other hand, the sharp bend in orientation of the estuary around Newport News, ~10 km to the south of the study area (Figure 1), may induce centrifugal accelerations that could influence the dynamics in the vicinity of the headland [e.g., *Geyer*, 1993; *Chant and Wilson*, 1997]. These effects would be manifested in the form of secondary flows consisting of near-surface normal flows away from and near-bottom normal flows toward the headland. As will be seen in Section 4, the study area must be far enough away from the direct influence of the headland because such secondary circulation pattern was not observed on the mean nor on the tidal flow.

The James River estuary is forced by the direct freshwater influence from James River discharges and by tides subject to spring-neap modulation. Mean annual river discharges gauged at Richmond, Virginia, peak in March at roughly 500 m^3/s and are weakest in August at 80 m^3/s [*Wood and Hargis*, 1971]. Longitudinal density gradients in the study area range between 0.2 and 0.5 σ_t/km [*Hepworth and Kuo*, 1989]. Tides and tidal currents are predominantly semidiurnal, and the three most energetic constituents are, in order of importance, M_2, N_2, and S_2, with the M_2 bearing ~80% of the total energy of the signal [*Browne and Fisher*, 1988]. Therefore spring-neap variations with monthly asymmetry (only one extreme spring and neap period per month) are expected for both tides and tidal currents.

3. Data collection and Processing

Two cross-estuary transects in the lower James River (Figure 1) were sampled throughout two spring (October 26-27) and two neap (November 2-3) tidal cycles in the fall of 1996. The purpose of the data collection was to repeat cross-estuary transects as often as possible to capture the intratidal variability of the distribution of the flow and density fields across the estuary. This allows the effective isolation of the tidal and subtidal signals from the records. With the restriction of traversing at mean speeds of 2.5 m/s (5 knots to ensure current velocity data quality), we could complete 4 km transects in 25-30 min. This allowed the sampling of two parallel transects separated by ~1 km in <1.5 hours. The dimensions of this sampling rectangle (~4 km by 1 km) allowed enough repetitions of the transect (at least eight) during one tidal cycle to assure good quality and repeatability of the time series used for the data analysis and permitted the determination of the along-estuary consistency of the cross-estuary structure from transect to transect, i.e., at least within a distance of 1 km.

Each 25 hour long sampling effort consisted of continuous velocity measurements and station density profiles obtained with a 600 kHz Broad Band RD Instruments acoustic Doppler current profiler (ADCP) and a Sea Bird (SBE-25) conductivity-temperature-depth (CTD) recorder, respectively. One small boat (<10 m long) with an ADCP and one with a CTD ran together along the sampling rectangle. For the purposes of nomenclature, transect 1 was to the southeast of transect 2. The ADCP was mounted looking downward on a small (roughly 1.2 m long) catamaran and towed to the side of the vessel. The instrument recorded velocity profiles averaged over 30 s, which gave a horizontal spatial resolution of ~75 m. The bin size for vertical resolution was 0.5 m, and the closest bin to the surface was located at nearly 2 m. Compass calibration and data correction were performed following *Joyce* [1989]. Navigation was carried out with differential Global Positioning System (GPS). In addition to the underway sampling, which provided spatial coverage, moored conductivity-temperature (CT) sensors (SeaBird SBE26 with Paroscientific Digiquartz pressure sensors of 45 psia) were deployed at both ends of transect 2 and rendered temporal coverage on the tide and salinity signals.

A right-handed coordinate system is adopted in this study. The x axis coincides with the along-estuary direction and is positive toward the head of the estuary. Looking into the estuary, the y axis is positive toward the left. The z axis is positive upward. The time series of current velocity profiles recorded at each point along each transect and at each depth consisted of 20 values for the spring tides cruise and 17 values for the neap tides cruise. These time series spanned two tidal cycles and were subject to least squares harmonic analysis on the semidiurnal and diurnal frequencies, only [e.g., *Valle-Levinson et al.*, 1998]. The analysis yielded five parameters, for the along-estuary flow component u and the across-estuary flow component v, at each grid point of an interpolated mesh of data with 100 m spacing in the horizontal and 0.5 m in the vertical. The along-estuary direction was identified as that of maximum tidal current variance for the entire cross section of the estuary. This direction also coincided with the midchannel line. The five parameters of each flow component were the subtidal flow (u_s, v_s), the amplitude (u_{a2}, v_{a2}) and phase $(u_{\theta 2}, v_{\theta 2})$ of the semidiurnal tidal constituents and the amplitude (u_{a1}, v_{a1}) and phase $(u_{\theta 1}, v_{\theta 1})$ of the diurnal tidal constituents. Then, the reconstructed synoptic signal at each grid point of the mesh can be written as

$$(u, v) = (u_s, v_s) + (u_{a2}, v_{a2}) \sin[\sigma_2 t + (u_{\theta 2}, v_{\theta 2})] + (u_{a1}, v_{a1}) \sin[\sigma_1 t + (u_{\theta 2}, v_{\theta 2})], \tag{1}$$

where σ_2 and σ_1 are the semidiurnal ($2\pi/12.42$ h) and diurnal ($2\pi/23.9$ h) frequencies, respectively, and t is time in hours from the beginning of the day of the sampling. The root-mean-squared error between the fit and the observations was typically <0.05 m/s, which indicated that the fits reproduced well the actual conditions of the period observed. The variability explained by the fits was consistently >90%. The addition of a quarter-diurnal ($2\pi/6.21$ h) frequency to the analysis produced minor modifications to the subtidal flows. These modifications were only restricted to the shallowest portion (<3 m), at the southernmost end of the transects. The inclusion of the quarter-diurnal frequency only increased by <1% the variability explained by the fits.

The salinity measurements were subject to the same type of analysis as the flow. The sampling rectangle was repeated 16 times during spring tides and 10 times during neap. During neap tides the salinity time series did not have as high temporal resolution as the current velocity measurements because of boat and instrument failures. Despite the increased sampling interval for salinity the root-mean-squared error between the fit and the observations was typically <0.2 and the variability explained by the fit was also consistently >90%.

The river discharge that influenced the area studied decreased by 15% from spring (130 m^3/s) to neap tides (110 m^3/s) [*Li et al.*, 1998]. These discharges were still higher than normal, as 1996 was the wettest year on record in terms of river discharge to the Chesapeake Bay and fourth wettest for the James River. The wind velocities remained below 10 m/s, which allowed the sampling of the transects from small boats.

4. Description of Observations

The subtidal salinity and flow fields are described first in the context of their cross-estuary variability from spring to neap tides. This spatial structure is then analyzed in the context of the variability of the main dynamic terms that arise from a scaling analysis of the subtidal transverse momentum equation.

4.1. Subtidal Salinity and Flow Fields

The mean salinity fields show distributions expected from the influence of Coriolis accelerations. Light water appears to the left (looking into the estuary), and heavy water is to the right (Figure 2). The influence of the Earth's rotation seems to be consistent from spring to neap tides. Nonetheless, neap tides feature stronger vertical stratification and larger range of salinities than those of spring tides as expected from reduced vertical mixing effects. The subtidal flows are also consistent with the fortnightly variability produced by tidal mixing (Figure 3). Along-estuary flows are stronger during neap tides than during spring tides. The bathymetric partition of the net flows, consisting of net inflows restricted to the channel and net outflows over the shoals as observed by *Wong* [1994] and *Valle-Levinson and Lwiza* [1995, 1997], does not develop clearly here (Figures 3 and 4). This is attributed to the location of the channel in the proximity to the right shore (looking into the estuary), which contains the net inflow and prevents development of outflow over the right portion of the cross section. This has been shown in the numerical results of *Valle-Levinson and O'Donnell* [1996].

Although the along-estuary subtidal flows are stronger during neaps than during springs, the cross-estuary flows are weaker during neaps (Figure 4). These transverse flows are mostly directed toward the right, although near the bottom of the ebb-dominated part of the main channel the transverse flow is consistently directed to the left. As discussed in Section 4.2., this pattern of transverse flows likely results from the mean barotropic pressure gradient, which is positive. On the basis of the fortnightly variability of the cross-estuary flow and salinity fields observed here it may be speculated that the momentum balance approaches geostrophy (as given by *Pritchard* [1956]) during neap tides and departs from geostrophy during spring tides. This speculation is suggested by the weak cross-estuary flows and apparent influence of the Coriolis accelerations during neaps and the well-developed cross-estuary flows during springs (Figure 4). This is now explored quantitatively by calculating the mean baroclinic pressure gradients and by comparing their magnitude to that of the main terms that stem from the following scaling analysis of the subtidal transverse momentum equation.

The tidally averaged (or subtidal) transverse momentum equation may be written as

$$\langle u\frac{\partial v}{\partial x}\rangle + \langle v\frac{\partial v}{\partial y}\rangle + \langle w\frac{\partial v}{\partial z}\rangle + \langle fu\rangle = -\langle\frac{1}{\rho_o}\frac{\partial p}{\partial y}\rangle + \langle\frac{\partial}{\partial z}(A_v\frac{\partial v}{\partial z})\rangle, \tag{2}$$

where the angle brackets denote tidal averages and where the tidally averaged horizontal friction has been neglected. In

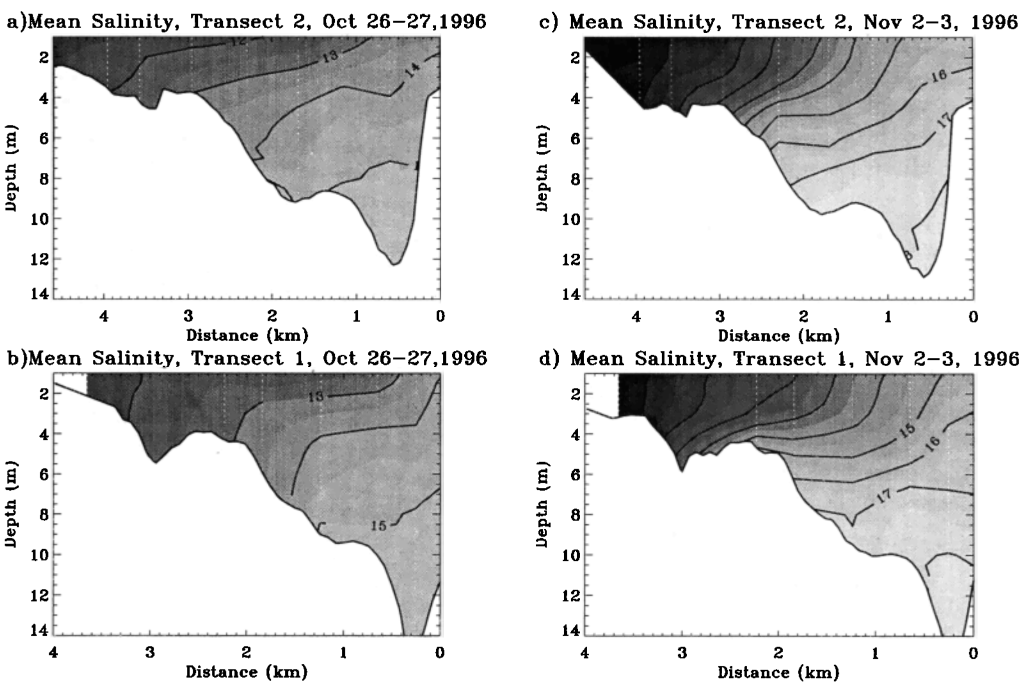

Figure 2. Average salinity across (a) transect 2 and (b) transect 1 over the spring tides of October 26-27, 1996, and (c) transect 2, and (d) transect 1 over the neap tides of November 2-3, 1996 (looking into the estuary). Values are contoured at intervals of 1 and color-filled at intervals of 0.5. The position of the CTD stations are at the ends of each transect and at the white dotted lines.

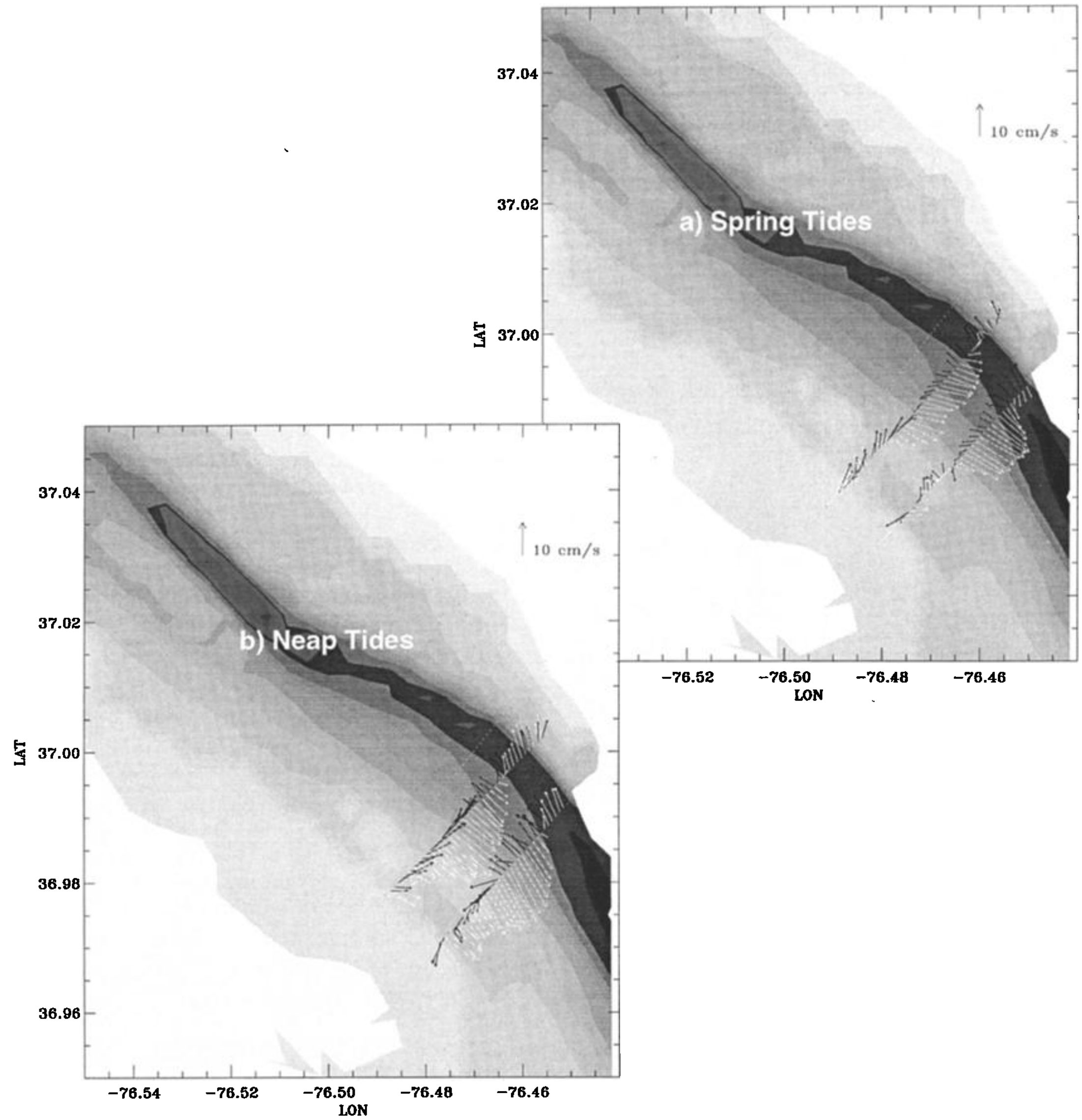

Figure 3. Subtidal flows during (a) spring tides and (b) neap tides, plotted over the bathymetry of the lower James River. White arrows denote surface flows, and dark arrows indicate near-bottom flows.

(2), f is the Coriolis parameter (8.8×10^{-5} s^{-1}), p is pressure (in Pa), ρ_0 is a reference density (~1010 kg/m^3 for the James River during the period of observations), and A_v is a space-time variable vertical eddy viscosity (in m^2/s). The balance expressed in (2) contains the influence of advective, Coriolis, and pressure gradient accelerations, as well as vertical exchange of momentum. The advective accelerations (first three terms on the left-hand side of (2)) have been included because the tidally averaged centripetal acceleration $\langle U^2/R\rangle$, where U is the current speed and R (= 10 km) is the radius of curvature of the bathymetry in the study area, is of the same order of magnitude as $\langle fu\rangle$. The term $\langle U^2/R\rangle$ represents the sum of the advective accelerations [*Doyle and Wilson*, 1978]. Scaling of (2) with the parameters shown in Table 1 suggests that the largest advective term is the one related to the convergence of lateral flow $\langle v\ \partial v/\partial y\rangle$, which has been referred to as the Bernoulli-type term [*Ott and Garrett*, 1998]. The size of this term can be determined with the observations in the James River. Retaining the terms of order 10^{-5} m/s^2 in (2) reduces it to

$$\langle v\frac{\partial v}{\partial y}\rangle + \langle fu\rangle = -\langle\frac{1}{\rho_o}\frac{\partial p}{\partial y}\rangle + \langle\frac{\partial}{\partial z}(A_v\frac{\partial v}{\partial z})\rangle. \tag{3}$$

The importance of each term of (3) relative to the pressure gradient is now assessed. In order to do that the pressure gradients are calculated first.

4.2. Pressure Gradients

The transverse baroclinic pressure gradients $\langle g/\rho\int_{-h}^{z}\partial\rho/\partial y\,dz\rangle$ are calculated with the density values derived from the CTD measurements. These gradients show a tendency to increase with depth and to produce flow from heavy to light water (Figure 5), as expected. The gradients have typical magnitudes of 1-2×10^{-5} m/s^2 during springs and 2-3×10^{-5} m/s^2 during neaps. Thus the baroclinic pressure gradients are typically <50% stronger during neaps relative to springs, which traditionally has been attributed to the fortnightly modulation of tidal mixing.

The transverse slopes of the surface elevation η determined from the de-meaned and detrended time series of the pressure sensors at either side of the estuary are similar from spring to neap tides at ~2×10^{-6}. These values are just above the accuracy limits of detection of the pressure sensors. Each sensor has an accuracy of 0.002 m so that any reliable difference between the two instruments must be >0.006 m in

Table 1. Scaling of Equation (2)

Term	Scaled Term	Value ($\times 10^{-5}$), m/s^2
$\langle u\frac{\partial v}{\partial x}\rangle$	UV/L_x	0.5
$\langle v\frac{\partial v}{\partial y}\rangle$	V^2/L_y	2.5
$\langle w\frac{\partial v}{\partial z}\rangle$	WV/H	0.25
$\langle fu\rangle$	fU	1
$\langle\frac{1}{\rho_o}\frac{\partial p}{\partial y}\rangle$	$g\alpha$	1
$\langle\frac{\partial}{\partial z}[A_v\frac{\partial v}{\partial z}]\rangle$	A_vV/H^2	1

The terms were scaled on the basis of the following values: $U = 0.1$ m/s; $V = 0.05$ m/s; $W = 1\times10^{-4}$ m/s; $L_x = 1000$ m; $L_y = 100$ m; $H = 2$ m; $f = 1\times10^{-4}$ s^{-1}; $A_v = 1\times10^{-3}$ m^2/s; $\alpha = 1\times10^{-6}$; $g = 10$ m/s^2. The parameters α and g denote the sea surface slope and the acceleration due to gravity, respectively. The rest of the variables are presented in the text.

4 km or a slope of 1.5×10^{-6}. The transverse barotropic pressure gradient $\langle g\partial\eta/\partial y\rangle$ resulting from the observed surface slope at springs and neaps is then 2×10^{-5} m/s^2. The positive value indicates that η increases toward the left (looking into the estuary) so that the pressure gradient force per unit mass is directed toward the right. This is reflected by the transverse mean flows directed mostly to the right (Figure 4). Then, the transverse mean flow appears to result from the competition between the barotropic and baroclinic pressure gradients because the transverse flow directed to the right is weaker during neaps, when the baroclinic pressure gradients are stronger, than during springs.

For comparison, the along-estuary baroclinic pressure gradients ($\langle g/\rho \int_{-h}^{z}\partial\rho/\partial x\, dz\rangle$) are also calculated with the density values and show a bathymetric partition consistent with *Wong*'s [1994] analytic results. The bathymetric partition should allow the development of inflow in the channel and outflow over shoals. Similar to the transverse gradients, the along-estuary baroclinic pressure gradients are stronger during neaps than during springs in the portion of the estuary studied. This is attributed to the increased mean advective flux of salt during neaps due to the enhanced along-estuary flow. The magnitude of the transverse baroclinic pressure gradient is now compared to the Coriolis accelerations, that of the nonlinear advection, and the vertical exchange of momentum to explore the validity of the geostrophic approximation for the transverse dynamics in a coastal plain estuary.

4.3. Coriolis Acceleration Versus Baroclinic Pressure Gradient

The magnitude of the ratio of the Coriolis accelerations $\langle fu\rangle$ to the transverse baroclinic pressure gradient $\langle g/\rho \int_{-h}^{z}\partial\rho/\partial y\, dz\rangle$ is, in general, <1 and typically ~0.2 (Figure 6). The ratios during neap tides appear even smaller than those during spring tides. This is due to a proportionally greater increase of $\langle g/\rho \int_{-h}^{z}\partial\rho/\partial y\, dz\rangle$ relative to $\langle fu\rangle$ from spring to neap tides. Only during spring tides and at

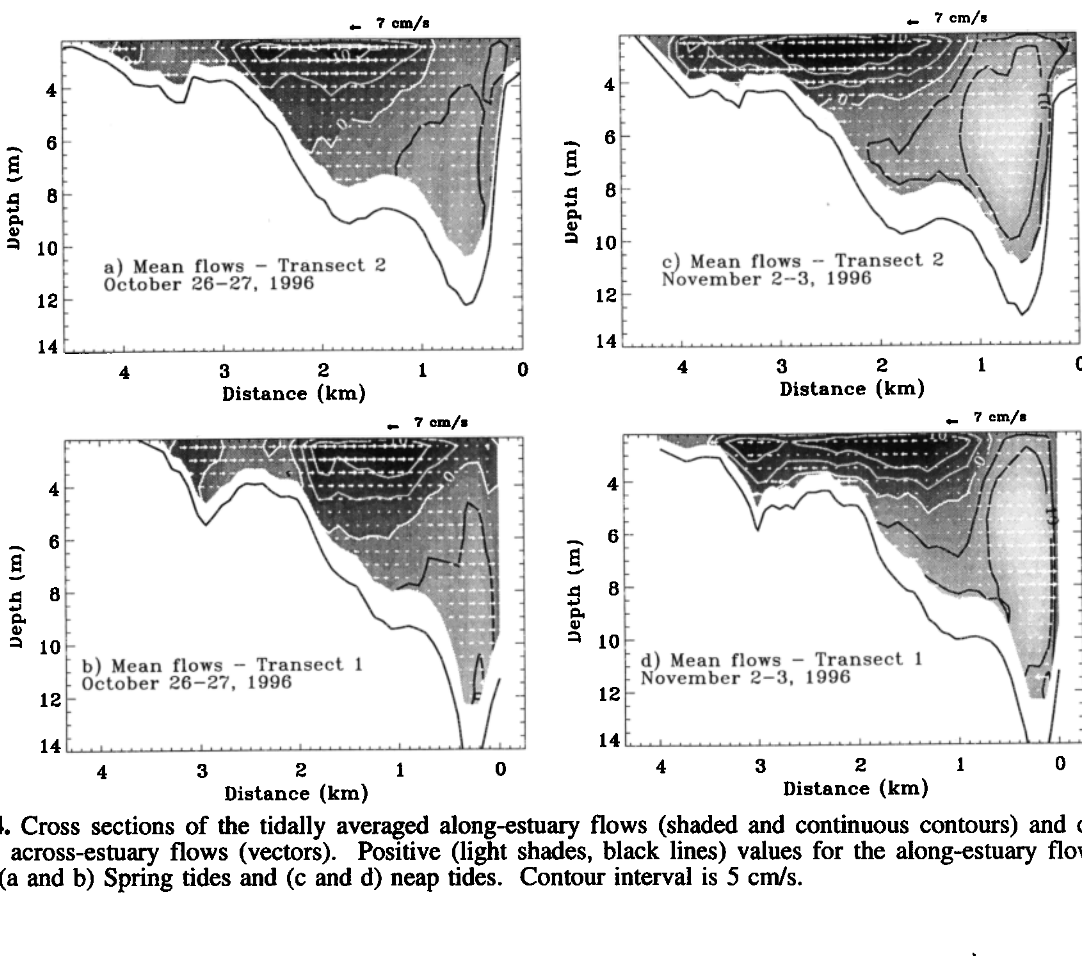

Figure 4. Cross sections of the tidally averaged along-estuary flows (shaded and continuous contours) and of the tidally averaged across-estuary flows (vectors). Positive (light shades, black lines) values for the along-estuary flow denote net inflow. (a and b) Spring tides and (c and d) neap tides. Contour interval is 5 cm/s.

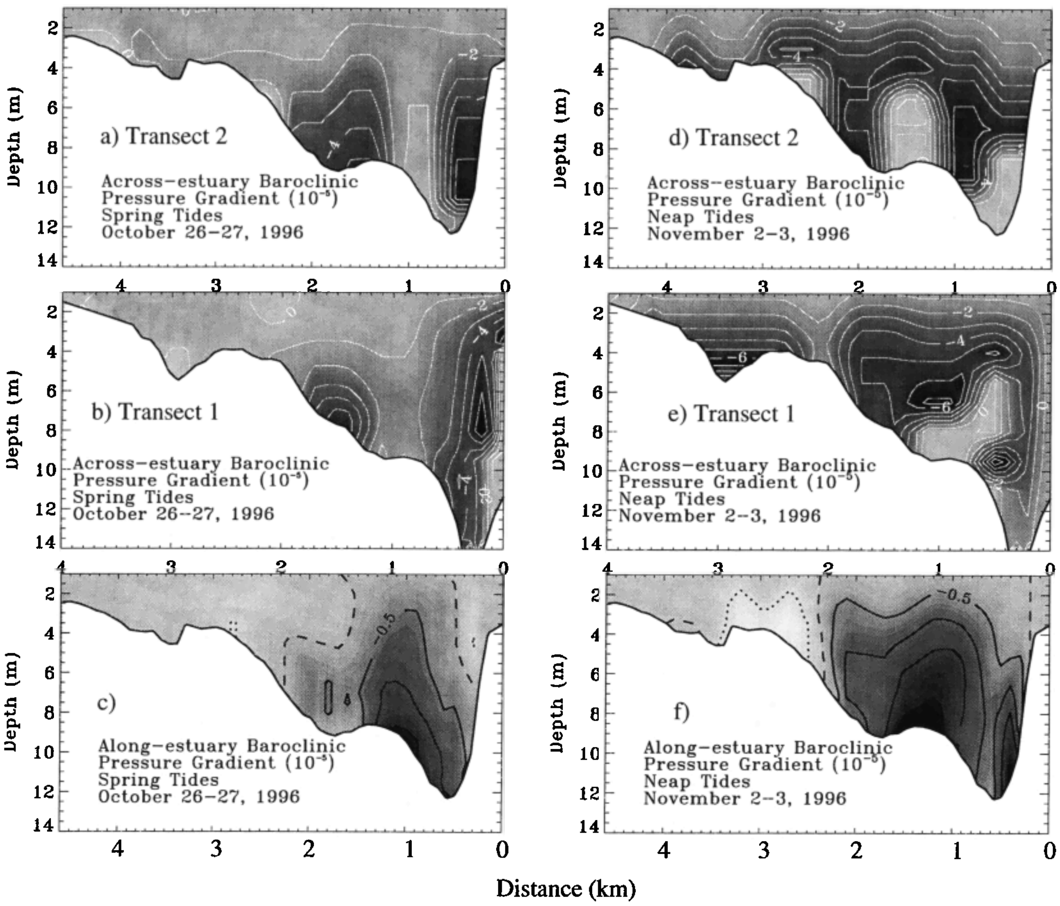

Figure 5. Baroclinic pressure gradients in the lower James River. (a and b) Across-estuary baroclinic pressure gradients and (c) along-estuary baroclinic pressure gradients in spring tides. (d and e) Across-estuary baroclinic pressure gradients and (f) along-estuary baroclinic pressure gradients in neap tides. Contour interval is 1.0×10^{-5} m/s^2 for the across-estuary gradients and 0.5×10^{-5} m/s^2 for the along-estuary gradients.

the surface over the shallow (ebb dominated) partition of the main channel is the magnitude of Coriolis accelerations comparable to that of the baroclinic pressure gradient (Figures 6a and 6b). There is also some indication that near the surface of the flood-dominated portion of the main channel the Coriolis accelerations are influential to the transverse dynamics. This area is where the near-surface subtidal transverse flow is weakest. Since $\langle fu \rangle$, in general, does not seem large enough to balance $\langle g/\rho \int_{-h}^{z} \partial\rho/\partial y\, dz \rangle$, additional accelerations are needed to produce the dynamic balance. In a study that focuses on the transverse gradients of the flow in the lower Chesapeake Bay, *Valle-Levinson and Atkinson* [1999] found that the nonlinearities produced by the Bernoulli-type advection term $\langle v\, \partial v/\partial y \rangle$ are between 0.2 and 10 times $\langle fu \rangle$. Therefore we now compute the magnitude of the ratio of $\langle v\, \partial v/\partial y \rangle$ to $\langle g/\rho \int_{-h}^{z} \partial\rho/\partial y\, dz \rangle$.

4.4. Advective Acceleration Versus Baroclinic Pressure Gradient

The magnitude of the ratio of $\langle v\, \partial v/\partial y \rangle$ to $\langle g/\rho \int_{-h}^{z} \partial\rho/\partial y\, dz \rangle$ is also, in general, <1 (Figure 7). Nonetheless, the nonlinear accelerations appear relevant over the channel edges, where the convergence of the transverse flow is most marked. Also, the ratio is smaller in neap tides than in spring tides owing to weaker nonlinearities derived from tidally rectified flow, i.e., the mean flow produced by tidal flows. This agrees with studies that point out that the tidally rectified flow is proportional to tidal forcing [e.g., *Li et al.*, 1998]. The distributions of the $\langle v\, \partial v/\partial y \rangle$ to $\langle g/\rho \int_{-h}^{z} \partial\rho/\partial y\, dz \rangle$ ratio also suggest that nonlinear advective accelerations alone are not large enough to balance the baroclinic pressure gradient. It is possible that both $\langle v\, \partial v/\partial y \rangle$ and $\langle fu \rangle$ have similar contribution to the momentum balance. This is now explored through the magnitude of the ratio of $\langle v\, \partial v/\partial y \rangle$ to $\langle fu \rangle$.

4.5. Advective Versus Coriolis Accelerations

The magnitude of the ratio of $\langle v\, \partial v/\partial y \rangle$ to $\langle fu \rangle$ shows regions of alternate dominance in each of these accelerations (Figure 8). In the region of surface net outflow, over the ebb-dominated partition of the main channel, Coriolis accelerations appear larger than nonlinear advection. The same is true in the region of net inflow within the flood-dominated partition, except in transect 1 during spring tides, when they are comparable. On the other hand, advective accelerations appear larger at the transition between net along-estuary inflow and net along-estuary outflow and over the edge of the channel. The large ratios are related to the combination of low values of $\langle u \rangle$ at these transition areas and the large intratidal convergences of lateral flow as shown by A. Valle-Levinson et al. (Convergence of lateral flow along a coastal plain estuary, submitted to *Journal of Geophysical Research*, 1999). The dominance of $\langle v\, \partial v/\partial y \rangle$ over $\langle fu \rangle$ at

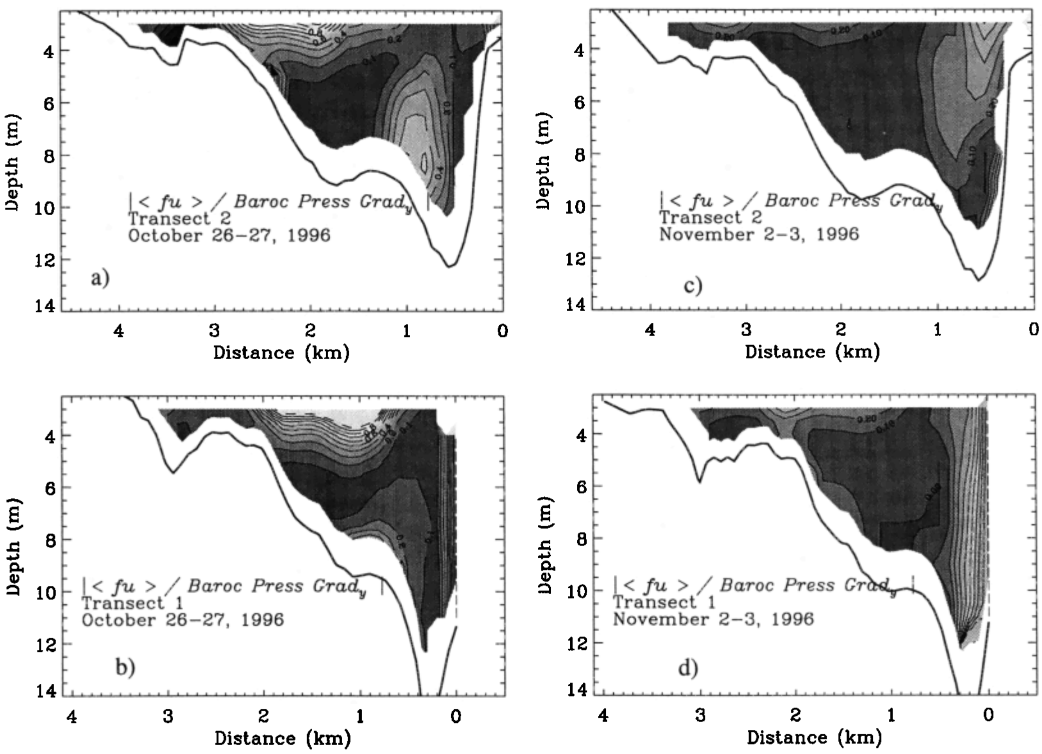

Figure 6. Absolute value of the ratio of the mean Coriolis accelerations to the mean baroclinic pressure gradient. (a and b) Spring tides and (c and d) neap tides. Contour interval is 0.1.

the edges of the channel and the dominance of $\langle fu \rangle$ over $\langle v\,\partial v/\partial y \rangle$ in the channel are consistent with the distributions observed in a wider system, the lower Chesapeake Bay, by *Valle-Levinson and Atkinson* [1999]. Although there are regions of nonlinear advective dominance and regions of Coriolis accelerations dominance, none are large enough to equilibrate the baroclinic pressure gradient. Other possible agents that should contribute to balance the baroclinic pressure gradient are frictional effects and the barotropic pressure gradient. As discussed in Section 4.2., the barotropic pressure gradient observed is of the same order of magnitude as the other terms that appear relevant to the momentum balance and therefore does influence the dynamics. The predominant direction of the tidally averaged transverse flow is consistent with the direction of the cross-estuary barotropic pressure gradient acceleration. It remains to be determined whether vertical exchange of momentum (friction) plays a role.

4.6. Vertical Exchange of Momentum

To determine whether frictional effects contribute effectively to the subtidal momentum balance, the intratidal frictional term $(\partial/\partial z[A_v\,\partial v/\partial z])$ needs to be calculated. This requires the use of a turbulent closure to determine the eddy viscosity coefficient A_v (e.g., a Richardson number-dependent scheme). The time- and space-dependent A_v is estimated for the springs and neaps cruises with the closure proposed by *Pacanowski and Philander* [1981]:

$$A_v = 0.01\,(1 + 5Ri)^{-2} + 10^{-4}, \tag{4}$$

where Ri is a gradient Richardson number that compares the stabilizing tendencies from the density stratification $(-g/\rho\,\partial\rho/\partial z)$ versus the destabilizing tendencies from vertical shears in the tidal flows $([\partial u/\partial z]^2 + [\partial v/\partial z]^2)$. This closure is chosen because it performs best among the low-order schemes [*Nunes Vaz and Simpson*, 1994].

The values of the tidally averaged eddy viscosity are, in general, $>5\times10^{-4}$ m^2/s outside of the main channel (Figure 9). This indicates increased frictional influences to the transverse momentum balance in shallow depths. During spring tides the largest values of $\langle A_v \rangle$ range between 15 and 20×10^{-4} m^2/s and are found close to the bottom in the ebb-dominated portion of the main channel (Figures 9a and 9b). At each location the values of $\langle A_v \rangle$ tend to increase with depth as bottom frictional influences become evident. In contrast, during neap tides, relatively large values of $\langle A_v \rangle$ ($10\text{-}15\times10^{-4}$ m^2/s) are found within the upper ~4 m of the water column (Figures 9c and 9d), consistent with the mean distribution of salinity (Figure 2) in the sense that the upper ~4 m show very weak mean salinity stratification. This near-surface band of increased $\langle A_v \rangle$ is a consequence of stronger winds (close to 10 m/s) relative to those prevailing during spring tides. Below the near-surface frictional band the values of $\langle A_v \rangle$ are lower than those during spring tides, as expected from weakened tidal forcing. The reduction of mean viscosities from spring to neap tides underneath ~4 m is better defined in transect 1, which has a deeper channel, than in transect 2. Therefore there is some evidence of decreased frictional effects from spring to neap tides. This decrease is somewhat obscured by wind stress.

The relevance of the mean divergence of the vertical exchange of momentum, $\partial/\partial z[A_v\,\partial v/\partial z]$, to the transverse momentum balance is assessed by comparing its magnitude to that of the baroclinic pressure gradient (Figure 10). During spring tides, there is a well-defined bathymetric partition of the frictional effects, relative to the baroclinic

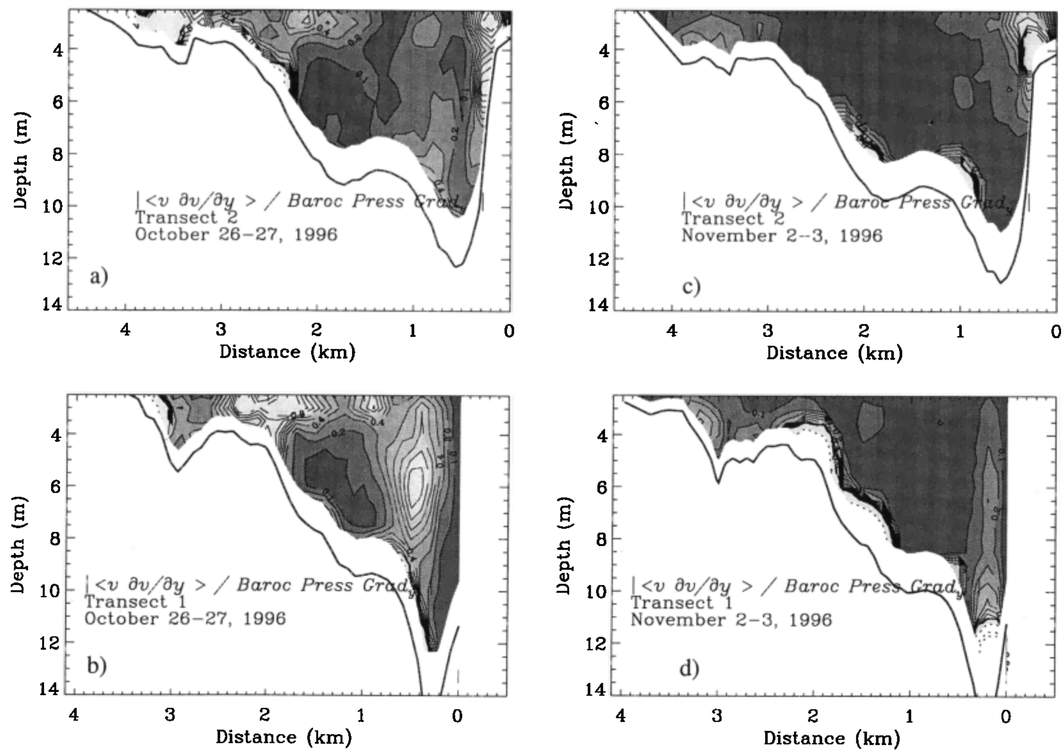

Figure 7. Absolute value of the ratio of the mean advective (Bernoulli-type) accelerations to the mean baroclinic pressure gradient. (a and b) Spring tides and (c and d) neap tides. Lighter tones denote higher ratios. Contour interval is 0.1.

effects (Figures 10a and 10b). In the flood-dominated portion of the main channel the frictional effects are typically 20% of the baroclinic effects. Elsewhere, frictional effects appear more important than, or at least as important as, the baroclinic effects. This suggests that friction is important to the springs transverse momentum balance over the shallow areas of the transect. During neap tides the bathymetric partition is not defined anymore as frictional influences decrease (Figures 10c and 10d). The area of increased ratios, between 0 and 200 m in transect 1 (Figure 10d), is related to very weak density gradients (Figure 5e). Outside of the near-surface band of increased $\langle A_v \rangle$ attributed to wind forcing, frictional effects represent a small fraction of the baroclinic pressure gradient and play a reduced role in the transverse dynamics, relative to spring tides.

For the development of theoretical models of estuarine dynamics it is valuable to determine the relative contribution to the mean vertical flux of horizontal momentum $\langle A_v \partial v/\partial z \rangle$ of its two components: (1) the product of $\langle A_v \rangle$ times $\partial \langle v \rangle/\partial z$, and (2) the covariance of the tidal fluctuations (denoted by primes) given by $\langle A_v' \partial v'/\partial z \rangle$. For both cruises and both sections the relative contribution of each component to the total vertical flux was at least 20%. This contribution changed in space and was roughly dominated by component 2 near the bottom throughout the section and in the channel. Elsewhere, it was dominated by component 1. In any case, both components are relevant to the mean vertical flux of momentum.

4.7. Implications of the Analysis

Calculation of each term of the transverse momentum balance presented in (3) produces errors or residuals of the order of 10^{-6} m/s^2. This is expected as the terms neglected from scaling of (2) are $<10^{-5}$ m/s^2. Therefore this analysis captures the main order of magnitude of the transverse dynamics in the James River from spring to neap tides. The analysis portrays the relevance of nonlinear advection and frictional effects in modifying the commonly used geostrophic dynamics. These modifications are more evident during spring tides because of stronger vertical mixing and greater nonlinearities in the tidal flows than during neap tides. The implication of the nongeostrophic nature of the transverse momentum balance is that there should be a redistribution of mass by the transverse flows. In the case of the James River estuary the lateral flow is mostly directed toward the deepest part of the channel, where dissolved and suspended material should tend to preferentially accumulate and/or deposit. This is a topic worthy of further investigation.

5. Summary

The main findings of this study of fortnightly variability in the transverse dynamics in the James River estuary, using measurements of current velocity and density profiles, are as follows. These all refer to tidally averaged properties: (1) The observed transverse baroclinic pressure gradients are larger than the along-estuary baroclinic pressure gradients and may play an important role in determining the strength of the along-estuary flow. (2) The transverse baroclinic pressure gradients are larger at neap tides than at spring tides due to decreased frictional influences. (3) Coriolis accelerations are not large enough to balance the transverse baroclinic pressure gradient. Other accelerations are required to produce a balance. (4) The Bernoulli-type of advective accelerations $\langle v \partial v/\partial y \rangle$ are at least as important as Coriolis accelerations and are greater at spring tides than at neap tides owing to greater nonlinearities induced by the tidal flow

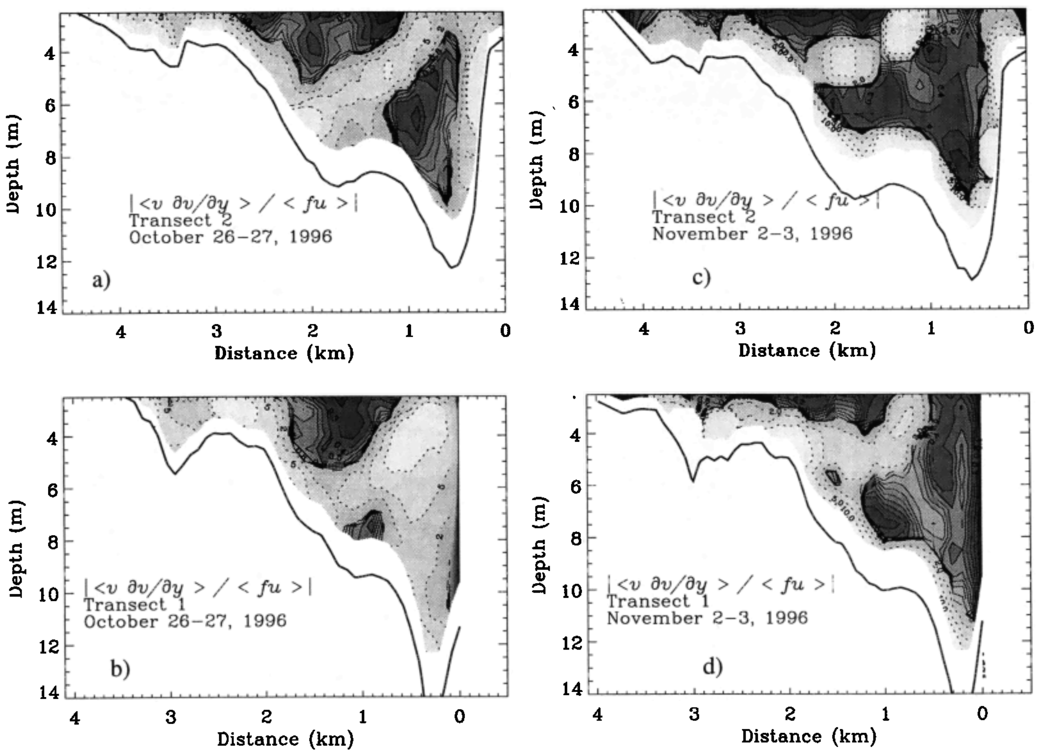

Figure 8. Absolute value of the ratio of the mean advective accelerations to the mean Coriolis accelerations. (a and b) Spring tides and (c and d) neap tides. Contour interval is 0.1 in the range 0-0.8 (continuous contours). Ratios equal to 1 are contoured with a dashed line. Ratios >1 (2, 5, 10) are denoted by light shading and dotted contours.

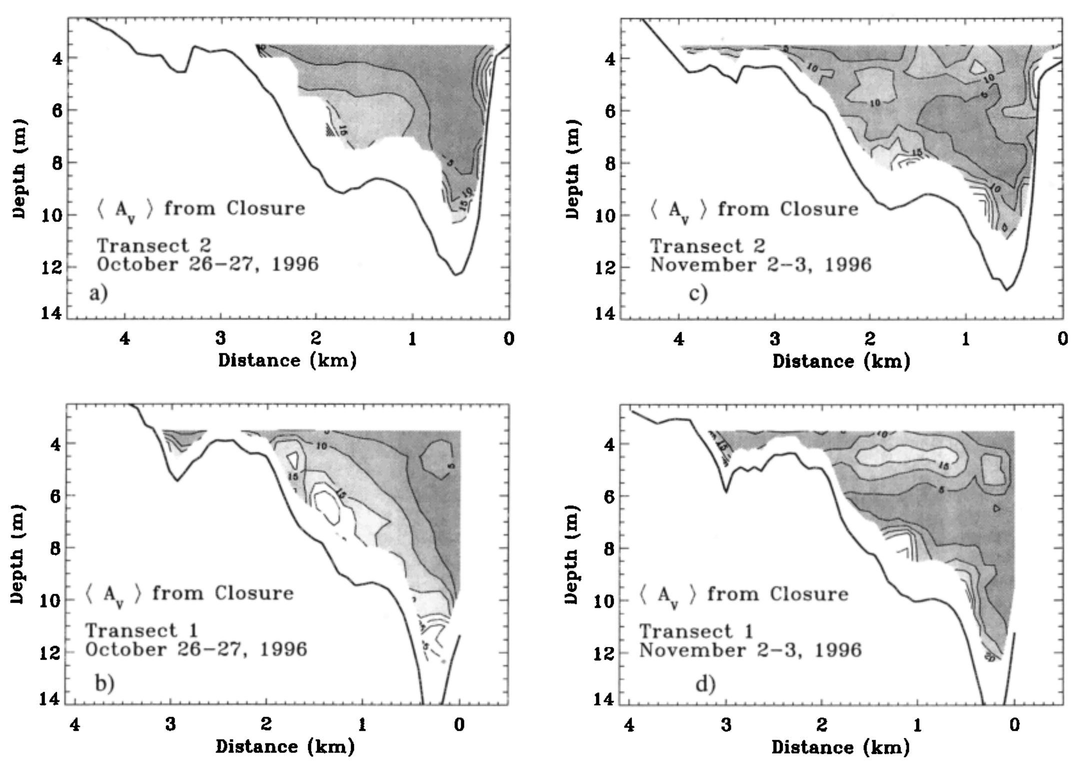

Figure 9. Tidally averaged eddy viscosities ($\times 10^{-4}$ m^2/s) calculated with the turbulence closure (4). (a and b) Spring tides and (c and d) neap tides. Contour interval is 5×10^{-4} m^2/s.

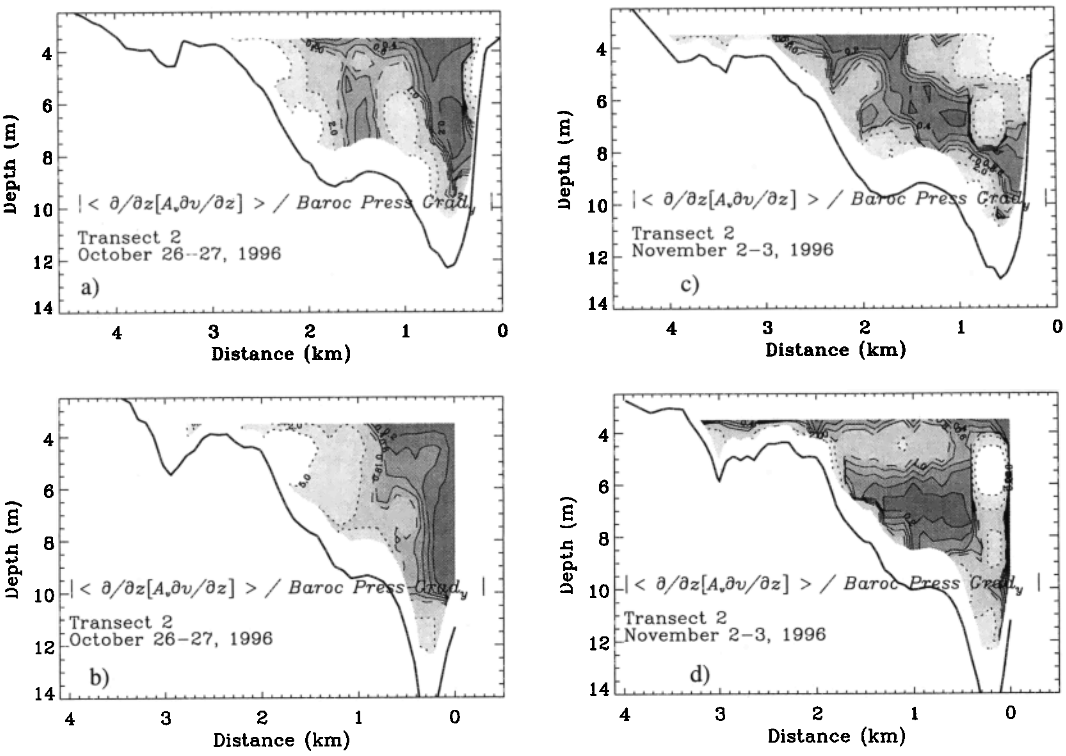

Figure 10. Absolute value of the ratio of the mean vertical exchange of momentum to the mean baroclinic pressure gradient. (a and b) Spring tides and (c and d) neap tides. Contour interval is 0.2 in the range 0-0.8 (continuous contours). Ratios equal to 1 are contoured with a dashed line. Ratios >1 (2, 5, 10) are denoted by light shading and dotted contours.

(stronger tidal rectification). (5) The transverse frictional influences are slightly more relevant at spring tides than at neap tides and are stronger in the shallow areas relative to the channel. (6) The main finding, which encompasses all of the above, is that the geostrophic approximation does not reflect adequately the transverse dynamics in relatively shallow partially stratified estuaries. The development of nonnegligible tidally averaged lateral flows, which should redistribute mass across the estuary, indicates that friction and nonlinear advection may also play a relevant role in the transverse dynamics of coastal plain estuaries.

Acknowledgments. This study was funded by the U.S. National Science Foundation through projects OCE-9529806, OCE-9530394, and OCE-9530395. Dozens of colleagues participated in the field work, and their help was invaluable. The assistance of R. Bray, R.C. Kidd, and W. Check with the operations on the field is specially appreciated. C. Friedrichs kindly encouraged us to estimate the eddy viscosities. The comments of two anonymous reviewers improved the manuscript and are greatly appreciated.

References

Bathurst, J.C., C.R. Thorne, and R.D. Hey, Direct measurements of secondary currents in river bends, *Nature, 269*, 504-506, 1977.

Browne, D.R. and C.W. Fisher, Tide and tidal currents in the Chesapeake Bay, NOAA Tech. Rep. NOS OMA 3, 143 pp., U.S. Dept. of Commerce, Rockville, Md., 1988.

Chant, R.J., and R.E. Wilson, Secondary circulation in a highly stratified estuary, *J. Geophys Res., 102*, 23,207-23,215, 1997.

Doyle, B.E., and R.E. Wilson, Lateral dynamic balance in the Sandy hook to Rockaway Point transect, *Estuarine Coastal Mar. Sci., 6*, 165-174, 1978.

Dronkers, J., The influence of buoyancy on transverse circulation and on estuarine dynamics, in *Buoyancy Effects on Coastal and Estuarine Dynamics*, Coastal Estuarine Stud., vol. 53, edited by David G. Aubrey and Carl T. Friedrichs, pp. 341-356, AGU, Washington, D.C., 1996.

Fischer, H.B., Mass transport mechanisms in partially stratified estuaries, *J. Fluid Mech., 53*(4), 671-687, 1972.

Fischer, H.B., Mixing and dispersion in estuaries, *Annu. Rev. Fluid Mech., 8*, 107-133, 1976.

Friedrichs, C.T., and J.M. Hamrick, Effects of channel geometry on cross-sectional variation in along channel velocity in partially stratified estuaries, in *Buoyancy Effects on Coastal and Estuarine Dynamics*, Coastal Estuarine Stud., vol. 53, edited by David G. Aubrey and Carl T. Friedrichs, pp. 283-300, AGU, Washington, D.C., 1996.

Geyer, W.R., Three-dimensional tidal flow around headlands, *J. Geophys. Res., 98*, 955-966, 1993.

Griffin, D.A., and P.H. LeBlond, Estuary/ocean exchange controlled by spring-neap tidal mixing, *Estuarine Coastal Shelf Sci., 30*, 275-305, 1990.

Haas, L.W., The effect of the spring-neap tidal cycle on the vertical salinity structure of the James, York and Rappahannock Rivers, Virginia, USA, *Estuarine Coastal Mar. Sci., 5*, 485-496, 1977.

Hepworth, D., and A.Y. Kuo, James River seed oyster bed project, Physical data report, I, 1984-1987, Data Rep. 31, Va. Inst. of Mar. Sci., Gloucester Pt., 1989.

Huzzey, L.M., and J.M. Brubaker, The formation of longitudinal fronts in a coastal plain estuary,. *J. Geophys. Res., 93*, 1329-1334, 1988.

Jay, D.A., and J.D. Smith, Circulation, density distribution and neap-spring transitions in the Columbia River Estuary., *Progr. Oceanogr., 25*, 81-112, 1990.

Joyce, T.M., On in situ calibration of shipboard ADCPs, *J. Atmos. Oceanic Technol., 6*(1), 169-172, 1989.

Kalkwijk, J.P.T., and R. Booij, Adaptation of secondary flow in nearly-horizontal flow, *J. Hydraul. Eng., 24*, 19-37, 1986.

Kjerfve, B., Bathymetry as an indicator of net circulation in well mixed estuaries, *Limnol. Oceanogr., 23*, 816-821, 1978.

Kjerfve, B., and J. A. Proehl, Velocity variability in a cross-section of a well-mixed estuary, *J. Mar. Res., 37,* 409-418, 1979.

Li, C., A. Valle-Levinson, K.C. Wong, and K.M.M. Lwiza, Separating baroclinic flow from tidally induced flow in estuaries, *J. Geophys. Res., 103,* 10,405-10,417, 1998.

Miller, J.L., and A. Valle-Levinson, Effects of Chesapeake Bay Bridge-Tunnel pilings on destratification in the lower Chesapeake Bay, *Estuaries, 19*(6), 526-539, 1996.

Nunes, R.A., and G.W. Lennon, Episodic stratification and gravity currents in a marine environment of modulated turbulence, *J. Geophys. Res., 92,* 5465-5480, 1987.

Nunes Vaz, R.A., and J.H. Simpson, Turbulence closure modeling of estuarine stratification, *J. Geophys. Res., 99,* 16,143-16,160, 1994.

Ott, M.W., and C. Garrett, Frictional estuarine flow in Juan de Fuca Strait, with implications for secondary circulation, *J. Geophys. Res., 103,* 15,657-15,666, 1998.

Pacanowski, R.C., and S.G.H. Philander, Parameterization of vertical mixing in numerical models of tropical oceans, *J. Phys. Oceanogr., 11,* 1443-1451, 1981.

Pritchard, D.W., Salinity distribution and circulation in the Chesapeake Bay estuarine system, *J. Mar. Res., 11,* 106-123, 1952.

Pritchard, D.W., A study of the salt balance in a coastal plain estuary, *J. Mar. Res., 13,* 133-144, 1954.

Pritchard, D.W., The dynamic structure of a coastal plain estuary, *J. Mar. Res, 15,* 33-42, 1956.

Simpson, J. H., J. Brown, J.P. Matthews, and G. Allen, Tidal straining, density currents and stirring in the control of estuarine stratification, *Estuaries, 12,* 125-132, 1990.

Thorne, C.R., and R.D. Hey, Direct measurements of secondary currents at a river inflexion point, *Nature, 280,* 226-228, 1979.

Valle-Levinson, A., and L. Atkinson, Spatial gradients in the flow over an estuarine channel, *Estuaries, 22,* 179-193, 1999.

Valle-Levinson, A., and K.M.M. Lwiza, The effects of channels and shoals on the exchange between the lower Chesapeake Bay and the adjacent ocean, *J. Geophys. Res., 100,* 18,551-18,563, 1995.

Valle-Levinson, A., and K.M.M. Lwiza, Bathymetric influences on hydrographic and flow distributions in the lower Chesapeake Bay, *J. Mar. Syst., 12,* 221-236, 1997.

Valle-Levinson, A., and J. O'Donnell, Tidal interaction with buoyancy driven flow in a coastal plain estuary, *Buoyancy Effects on Coastal and Estuarine Dynamics*, Coastal Estuarine Stud., vol. 53, edited by David G. Aubrey and Carl T. Friedrichs, pp. 265-281, AGU, Washington, D.C., 1996.

Valle-Levinson, C. Li, T. Royer, and L. Atkinson, Flow patterns at the Chesapeake Bay entrance, *Cont. Shelf Res., 18*(10), 1157-1177, 1998.

Wong, K.-C., On the nature of transverse variability in a coastal plain estuary, *J. Geophys. Res., 99,* 14,209-14,222, 1994.

Wong, K.-C., and A. Münchow, Buoyancy forced interaction between estuary and inner shelf: Observation, *Cont. Shelf Res., 15*(1), 59-88, 1995.

Wood, L., and W.J. Hargis, Transport of bivalve larvae in a tidal estuary, in *Proceedings 4th European Marine Biology Symposium*, edited by D.J. Crisp, pp. 29-44, Cambridge Univ., London, 1971.

K.M.M. Lwiza, Marine Sciences Research Center, State Univeristy of New York, Stony Brook, NY 11794.

A. Valle-Levinson, Center for Coastal Physical Oceanography, Department of Ocean, Earth, and Atmospheric Sciences, Old Dominion University, Norfolk, VA 23529. (arnoldo@ccpo.odu.edu).

K.-C. Wong, College of Marine Studies, University of Delaware, Newark, DE 19716.

(Received December 30, 1998; revised August 31, 1999; accepted October 14, 1999.)